Naval Research Laboratory
Washington, DC 20375-5320

NRL/6360/MR—2023/1

The Metal-Insulator Transition as a Tool for Materials by Design

MICHAEL OSOFSKY

Materials Physics and Chemistry Section
Materials Science and Technology Division

January 17, 2023

REPORT DOCUMENTATION PAGE

Form Approved
OMB No. 0704-0188

1. REPORT DATE *(DD-MM-YYYY)*	**2. REPORT TYPE**	**3. DATES COVERED** *(From - To)*
17-01-2023	NRL Memorandum Report	01/10/2018 – 09/30/2022

4. TITLE AND SUBTITLE

The Metal-Insulator Transition as a Tool for Materials by Design

5a. CONTRACT NUMBER

5b. GRANT NUMBER

5c. PROGRAM ELEMENT NUMBER
61153N

6. AUTHOR(S)

Michael Osofsky

5d. PROJECT NUMBER

5e. TASK NUMBER

5f. WORK UNIT NUMBER
1J05

7. PERFORMING ORGANIZATION NAME(S) AND ADDRESS(ES)

Naval Research Laboratory
4555 Overlook Avenue, SW
Washington, DC 20375-5320

8. PERFORMING ORGANIZATION REPORT NUMBER

NRL/6360/MR--2023/1

9. SPONSORING / MONITORING AGENCY NAME(S) AND ADDRESS(ES)

Naval Research Laboratory
4555 Overlook Avenue, SW
Washington, DC 20375-5320

10. SPONSOR / MONITOR'S ACRONYM(S)
NRL

11. SPONSOR / MONITOR'S REPORT NUMBER(S)

12. DISTRIBUTION / AVAILABILITY STATEMENT

DISTRIBUTION STATEMENT A: Approved for public release; distribution is unlimited.

13. SUPPLEMENTARY NOTES

14. ABSTRACT

We determine the influence of the universal electronic behavior (i.e., independent of the structural and chemical details of the material) near the metal–insulator transition (MIT) on the properties of functional materials such as superconductors and two-dimensional systems. Since many of the functional materials that are important for future naval applications, such as superconductors and dilute magnetic semiconductors, have been demonstrated to have metal-insulator transitions this program will provide a framework for predicting properties that cannot be accurately described by conventional methods such as band theory. The results of this program confirmed that conventional approaches to describing and predicting properties of functional materials with conductivities near the metal-insulator transition (MIT) must be complimented with those of the unconventional properties of the MIT. These include, superconductive, electronic transport, thermoelectric and electrocatalytic properties.

15. SUBJECT TERMS

Metal-insulator transition
Electronic transport
Superconductivity
Electrocatalytic properties
Thermo-electrics

16. SECURITY CLASSIFICATION OF:			**17. LIMITATION OF ABSTRACT**	**18. NUMBER OF PAGES**	**19a. NAME OF RESPONSIBLE PERSON**
					Michael Osofsky
a. REPORT	**b. ABSTRACT**	**c. THIS PAGE**	U	19	**19b. TELEPHONE NUMBER** *(include area code)*
U	U	U			(202) 767-6149

Standard Form 298 (Rev. 8-98)
Prescribed by ANSI Std. Z39.18

This page intentionally left blank.

CONTENTS

This page intentionally left blank.

EXECUTIVE SUMMARY

We determine the influence of the universal electronic behavior (i.e., independent of the structural and chemical details of the material) near the metal–insulator transition (MIT) on the properties of functional materials such as superconductors and two-dimensional systems. Since many of the functional materials that are important for future naval applications, such as superconductors and dilute magnetic semiconductors, have been demonstrated to have metal-insulator transitions this program will provide a framework for predicting properties that cannot be accurately described by conventional methods such as band theory. The results of this program confirmed that conventional approaches to describing and predicting properties of functional materials with conductivities near the metal-insulator transition (MIT) must be complimented with those of the unconventional properties of the MIT. These include, superconductive, electronic transport, thermoelectric and electrocatalytic properties.

This page intentionally left blank.

THE METAL-INSULATOR TRANSITION AS A TOOL FOR MATERIALS BY DESIGN

1. INTRODUCTION

We present here the closeout report on our program, *The Metal-Insulator Transition as a Tool for Materials By Design*. The goal of this program was to determine the influence of the universal electronic behavior (i.e., independent of the structural and chemical details of the material) near the metal–insulator transition (MIT) on the properties of functional materials such as superconductors and two-dimensional systems. Since many of the functional materials that are important for future naval applications, such as superconductors and dilute magnetic semiconductors, have been demonstrated to have metal-insulator transitions this program will provide a framework for predicting properties that cannot be accurately described by conventional methods such as band theory.

2. SUPERCONDUCTIVITY

Our previous work demonstrated that there is a universal dependence of the superconductive transition temperature, T_c, and proximity to the metal-insulator transition (MIT) as shown in figure 1 [1]. The MIT is the condition where the conductivity, σ, as the temperature approaches 0K is 0 $(\Omega\text{-cm})^{-1}$. As part of that work, a phenomenological model was developed to describe the peaked behavior of the data. A goal of the program was to identify the factors that influence the maximum T_c, T_{cMax}.

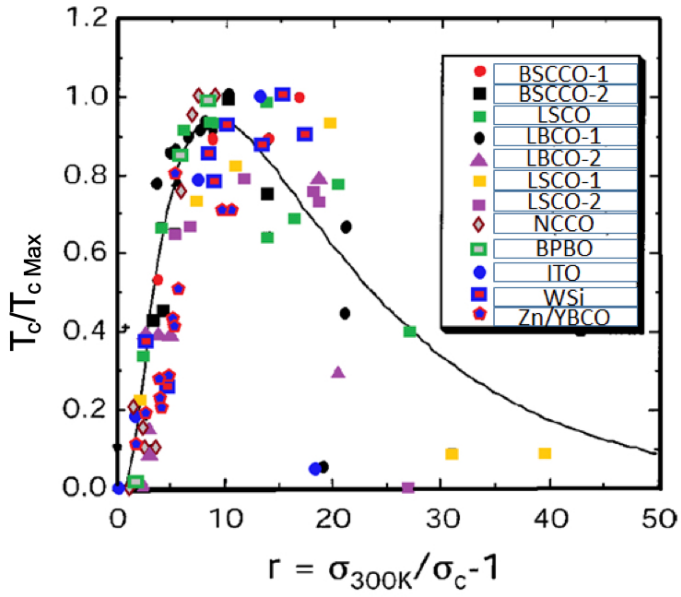

Fig. 1 — Behavior of T_c for various low and High T_c superconductors near the MIT (r=0) where r is a parameter characterizing the distance to the MIT. The solid line is a fit from a phenomenological model.

Manuscript approved January 12, 2023.

By considering a variant the well-known BCS equation for T_c

$$kT_c = 1.13\hbar\omega_c e^{-\frac{1}{N(0)V}} \quad (1)$$

where V can be expressed as

$$V(\vec{q},\omega) = \frac{4\pi e^2}{q^2 \varepsilon_{eff}(\vec{q},\omega)} \quad (2)$$

where N(0) is the single particle electron density of states and $\varepsilon_{eff}(q,\omega)$ is an effective dielectric function we realized that $\varepsilon_{eff}(q,\omega)$ is an important parameter for controlling T_{cMax}.

Over the past few years we demonstrated that a metamaterial approach to dielectric response engineering for enhancing T_c has been demonstrated in several systems [2-4]. This approach is based on an effective medium model where $\varepsilon_{eff}(q,\omega)$ is manipulated to enhance the electron-electron attraction through the use of nanoscale components with positive and negative dielectric responses and sizes that are less than the superconductive coherence length, ξ. This situation is analogous to that of systems near the MIT in that the dielectric response of the systems vary from that of an insulator (positive) to that of a metal (negative). Thus, a series of studies of well metamaterial systems with well controlled dielectric properties and enhanced superconductive properties were undertaken.

Our previous work showed that the T_c of Al/Al_2O_3 nano-shell composites was enhanced by over 3x compared to bulk Al. Furthermore, the dielectric response, which was extracted from optical reflectivity measurements, proved that the systems satisfied the epsilon near zero (ENZ) condition which, according to equations (1) and (2) explains the enhanced T_c. There are two key parameters in the BCS theory of superconductivity, the single particle density of states (DOS) and the attractive potential, V, which is due to the electron-phonon interaction in conventional superconductors. The enhancement of either would cause an increase of T_c. To further elucidate which is responsible for the observed enhancement, specific heat measurements, from which the DOS can be inferred, and inelastic neutron diffraction measurements, from which the phonon spectrum can be obtained, were performed with collaborators. The specific heat measurements clearly showed that the DOS that the Debye Temperature and electronic density of states are similar to that of pure aluminum and not enhanced in the composite sample. Since the T_c of a conventional low temperature superconductor is determined by the Debye Temperature and the coupling strength, which is expressed as the product of the single particle density of state (DOS) at the Fermi energy and an attractive electron-electron potential, these results confirm that the source of the T_c enhancement is indeed a modification of the attractive electron-electron interaction. Furthermore, the neutron diffraction studies found a predicted pole at an energy below the lowest known phonon energy of pure Al. Such a feature was shown to be consistent with a hybrid plasmon-phonon excitation. This low energy excitation is consistent with tunneling data in the literature. The lack of enhanced Debye temperature and electronic density of states coupled with the presence of the new plasmon-phonon excitation implies the existence of new mechanism responsible for the observed enhanced T_c and explains a 50+ year mystery.

Studies of tin-based metamaterial superconductors in the homogeneous, ENZ and layered, hyperbolic metamaterial configurations were performed. It was observed that, as expected, T_c enhancement is significantly reduced when the metamaterial structural dimensions exceed 240 nm, the superconducting coherence length in pure tin.

Since the theory of metamaterial superconductivity predicts that T_c should be enhanced by orders of magnitude in carefully grown dielectric/superconductor layered structures, the superconducting properties of sputtered Al/Al_2O_3 bilayer films with well controlled thicknesses were studied. The long coherence length of Al (~160 nm) makes this system ideal for basic studies. Furthermore, sputtering is

much more controlled than the thermal evaporation process used in the initial studies that showed a ~3x enhancement of the T_c of Al. The temperature dependent resistance of the following samples was obtained: (2 nm Al_2O_3)/(10 nm Al)/sapphire and (1 nm Al_2O_3)/(10 nm Al)/sapphire. There was no observed enhancement of the Al T_c (1.2K in bulk) above the measurement limit of ~1.8K for the first sample. There was an onset T_c at ~2K for the second sample indicating that the metamaterial enhancement can occur even for dielectric/metal bilayer structures.

The transport and optical properties of high-quality multilayers of NbTiN/AlN with ultrathin NbTiN layers were characterized. The anisotropy of the dielectric function of the multilayers confirmed their hyperbolic metamaterial properties. The superconductive transition temperature, T_c, of these engineered superconductors was enhanced up to 32% compared to the T_c of a single ultrathin NbTiN layer. We have demonstrated that this T_c increase can be attributed to enhanced electron-electron interaction in superconducting hyperbolic metamaterials. Studies of T_c vs. applied magnetic field showed that the critical fields in these multilayers are high and have anomalous linear temperature dependence in the perpendicular to the magnetic field direction, which can be attributed to disorder. These results demonstrate that the metamaterial approach to superconductor engineering can enable the increase the upper critical field, H_{c2}, as well as T_c. Since H_{c2} is an important property for power applications this result is important because it demonstrates that both T_c and magnetic properties can be engineered.

A combinatorial study of the transport and magnetic properties of Fe(x)B(1-x) thin films in the literature demonstrated that a phase spread of disordered Fe(x)B(1-x) exhibits ferromagnetic metallic behavior on the Fe rich side, the loss of ferromagnetism as the MIT is approached (with increased B content), the appearance of superconductivity closer to the MIT (with even greater B content), and insulating behavior on the B rich side. This entirely unexpected result opened the question of the mechanism for such behavior and showed that the FeB system is an ideal model system for the study of magnetism and superconductivity near the MIT. Since it is expected that the ENZ condition is satisfied near the MIT, Fe-B compositional spreads were prepared by co-sputtering onto a non-rotating intrinsic Si substrate with Fe and B targets located across from each other for studies of the dielectric properties. Indeed, the measurements showed that the ENZ condition is present in films near the MIT (figure 2).

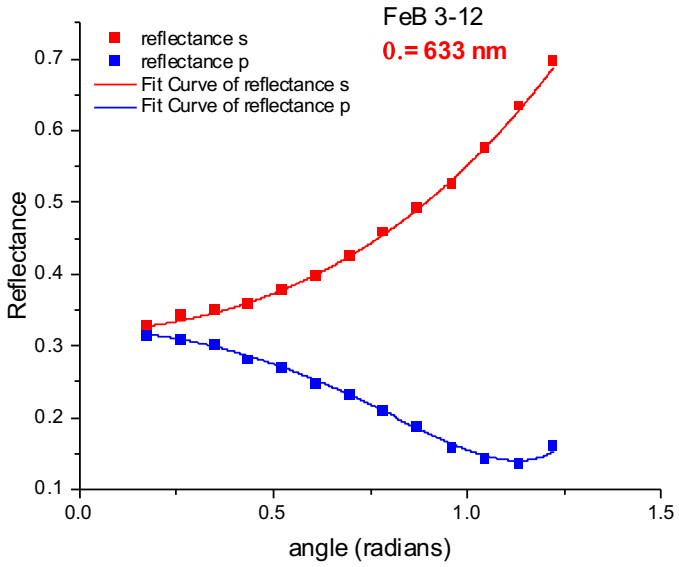

Fig. 2 — Reflectance of 633nm radiation with the polarization parallel and perpendicular to the surface of an FeB film near the MIT. The curves are fits of the data for ε=-0.0756.

3. USING THE MIT TO OPTIMIZE THERMOELECTRIC AND ELECTROCATALYTIC PROPERTIES OF RUO_2 NANOSKINS

Ruthenia (RuO_2) nanoskins, prepared by a solution-based, non-line-of sight deposition, undergo a continuous 2D metal-insulator transition (MIT) [5]. The RuO_2 nanoskins are an atypical 2D metal oxide with high carrier concentration but low carrier mobility. The films are highly disordered post-deposition and become more ordered and more metallic with increasing calcination temperature. The electrical conductivity and degree of order/disorder in RuO_2 nanoskins can be readily tuned, and the structure-dependent properties of RuO_2 nanoskins have been empirically optimized for applications including electrochemical capacitors [6, 7], Li-ion insertion anodes [8], chlorine oxidation [9], and oxygen evolution reaction [10]. Although the optimal RuO_2 structure differs for each of the aforementioned applications, the most active phase is usually near its MIT in a difficult to define structural regime blending order and disorder. We now explore how the electrocatalytic activity and thermoelectric properties of RuO_2 nanoskins are impacted by the orders of magnitude changes in carrier density and carrier mobility near the MIT and use the "r" parameter as a quantitative descriptor for where these behaviors are optimized.

We compare the electronic conductivity (σ), Seebeck coefficient (S), and power factors of 3-layer thick RuO_2 nanoskins ($3xRuO_2$) calcined at different temperatures (Figure 3). At calcination temperatures $\leq$ 200°C, the nanoskins show no long-range order beyond a radial distance of 8 Å, but at calcination temperatures $\geq$ 200°C, the nanoskins start to display some long-range order and show increased nanocrystalline rutile RuO_2 content [11]. The more ordered films are more conductive than the disordered films calcined at lower temperature (100 and 150°C, (Figure 3a). The RuO_2 films calcined at 200 and 250°C display metallic behavior (decreasing σ with increasing temperature) while the films calcined at 100 and 150°C behave as semiconductors with thermally activated conductivity. The Seebeck coefficient of RuO_2 nanoskins is higher for the disordered, non-metallic films (Figure 3b). Although they have fewer carriers than the ordered/metallic films, the mobile carriers possess higher energy, resulting in a higher Seebeck coefficient. The maximum Seebeck coefficient for RuO_2 nanoskins exceeds that of bulk RuO_2 films [12, 13]. The disorder and nanocrystallinity in the nanoskins may selectively scatter low energy carriers.

The power factor of RuO_2 nanoskins increases with increasing calcination temperature from 100 to 150°C, and then decreases with increasing calcination temperature up to 250°C (Figure 3c). Although the 100°C calcined film has a high Seebeck coefficient, its power factor suffers because of its poor σ. Although the 150°C calcined nanoskin has modest σ, its high Seebeck coefficient results in an optimum power factor. While the 100°C and 150°C calcined nanoskins may appear structurally similar by most traditional characterization methods, their electronic and thermoelectric properties clearly differ in significant ways. The powerfactor or the RuO_2 nanoskins is optimized at 150°C, which is the temperature at which their 2D transport behavior begins the transition from "strongly localized insulators" to "weakly localized carriers." Calcining above this temperature, the 2D transport behavior then transitions from "weakly localized carriers" to metallic conductance. Therefore, rather than relying on hard-to-define descriptions of structural order, the MIT can be used as a tool to identify where thermoelectric properties of thin films are optimized. We expect thermoelectric behavior of other materials to be similarly optimized near the MIT.

The electrocatalytic properties of RuO_2 also show dramatic changes near the MIT where the protonic and electronic conductivity of the RuO_2 nanoskins undergoes orders-of-magnitude changes. As they are thermally heated through the MIT, the RuO_2 nanoskins undergo a transition from a hydrous phase to an anhydrous phase. The as-deposited nanoskins likely exist as a mixture of RuO_2 and as metastable Ru_2O_3 phase intercalated with water and protons,[Error! Bookmark not defined.] contributing to the protonic functionality of the mixed electron-proton conductive hydrous phase. This type of mixed electron-proton conduction is important for electrochemical applications including charge storage and electrocatalysis. Optimization of RuO_2 for electrochemical applications is usually performed by an empirical balance between the two types of conduction, and we now look at electrocatalytic activity of RuO_2 nanoskins near the MIT.

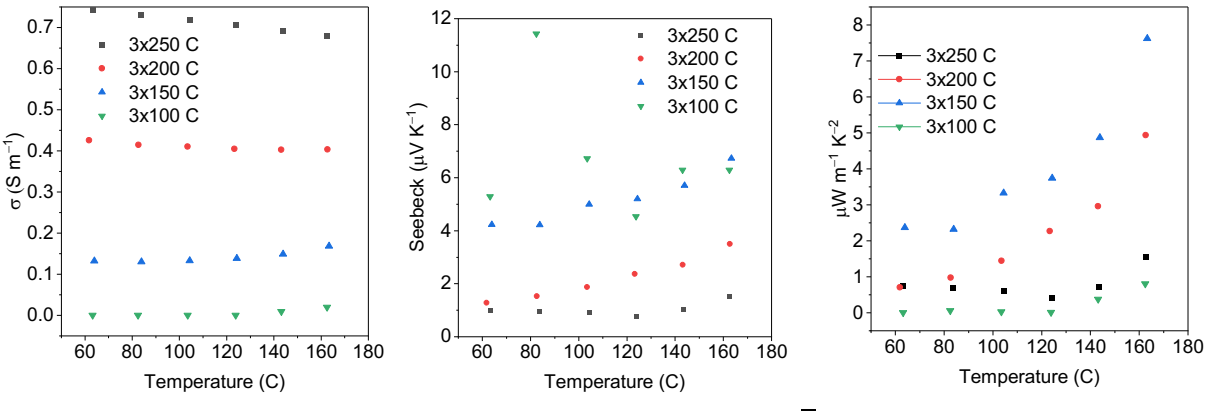

Fig. 3 — (a) Seebeck coefficient, (b) conductivity, and (c) power factor vs. temperature for 3-layer RuO_2 nanoskins calcined at different temperatures.

We characterize electrocatalytic activity for the oxygen evolution reaction (OER) and the hydrogen evolution reaction (HER) for 5-layer thick RuO_2 nanoskins ($5xRuO_2$) calcined at varying temperatures (Figure 4). As calcination temperature increases and the nanoskins convert to more of the anhydrous rutile phase, we see increased overpotential needed to achieve a current density of 1 mA/cm^2 for HER. The apparent loss in proton conductivity appears to limit the HER activity.

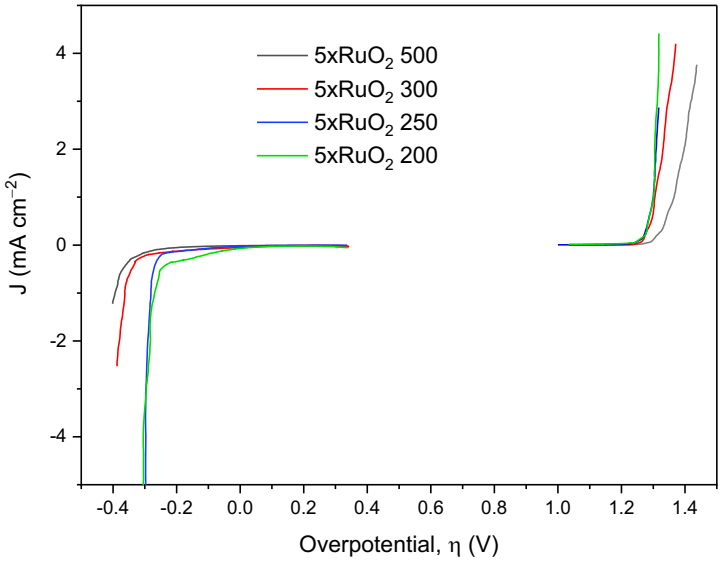

Fig. 4 — Current density (J) vs. overpotential for oxygen evolution and hydrogen evolution at 5-layer thick RuO_2 nanoskin electrodes in 0.1 M HCl.

In contrast, the RuO_2 nanoskin electrode calcined at 250°C achieves the best OER activity, suggesting that trading off protonic conductivity for electronic conductivity is beneficial for OER. However, although the films continue to increase in electronic conductivity at calcination temperatures ≥250°C, their OER activity is diminished, revealing that electronic conductivity is not the only factor limiting this electrocatalytic reaction. The bifunctional behavior of the nanoskins for overall water splitting—the combined overpotential to achieve both 1 mA/cm^2 of HER and OER—is optimized at a

calcination temperature of 250°C (Δ = 1.570 V). At this calcination temperature, the RuO_2 nanoskins show metallic 2D electronic transport behavior, however, they are still somewhat disordered and hydrous and thus possess a blend electronic and protonic conductivity which manifests in excellent electrocatalytic activity. Rather than rely on empirical optimization of order/disorder and protonic/electronic conductivity, the MIT transition to a 2D metal can be used to predict where electrocatalytic activity is optimized.

4. HIGH RESISTANCE AND HIGH FREQUENCY MEASUREMENT SYSTEMS

In order to study the magneto-transport properties of materials throughout the entire phase space of the metal-insulator transition (MIT), a unique system that interfaces with the Dynacool Physical Property Measurement System (PPMS) to perform 4-probe electrostatic gating measurements on samples with resistances ranging from 2μΩ – 200TΩ at T = 2 – 400K and H = ±9T was constructed. In particular, it enables intrinsic property extraction from the channels of 2D and thin film materials with naturally high contact resistance due to Schottky barriers (e.g. MoS_2) or those with poor metal adhesion (e.g. graphene). As a test of its capabilities the probe was used to measure the intrinsic transport properties of undoped Si to record low temperatures. Figure 5 shows the I-V sweep for two and four probe measurements of the Si demonstrating the non-Ohmic behavior of the contacts as measured in the two-probe configuration and the ability of the system to obtain Ohmic behavior in the four-probe measurement. Such measurements are not possible using standard measurements in very high resistance samples due to the Schottky barriers at the Si/metal contact interfaces. Interestingly, metallic transport behavior was observed from 400K down to ~250K, below which highly insulating behavior could be tracked down to 100K (figure 6). This is a new phenomenon that can be explained by the transport model described in the theory section below.

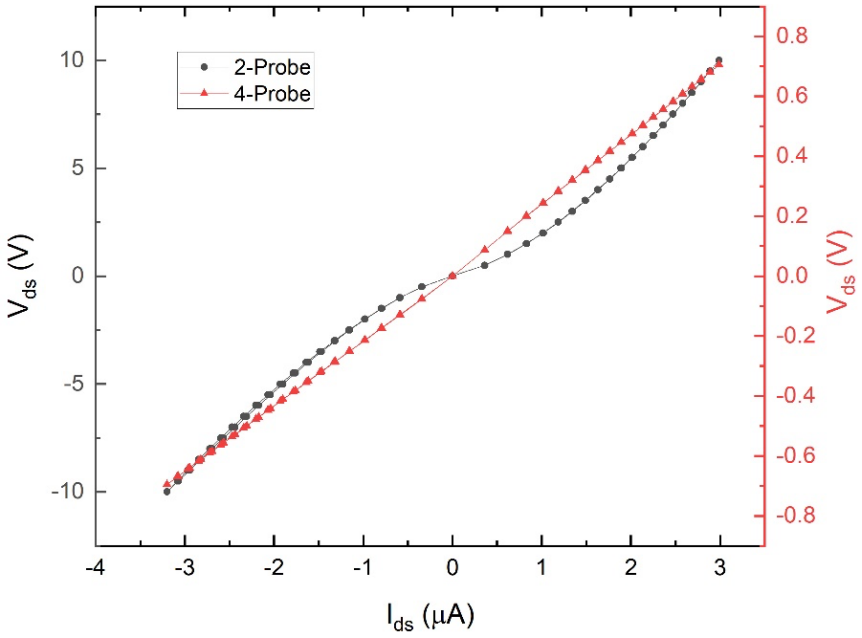

Fig. 5 — Bulk intrinsic silicon single crystal on UHR sample platform. UHR system capable of observing linear IV on rectifying sample using 4-probe measurements where conventional 2-probe high resistance measurement is non-linear.

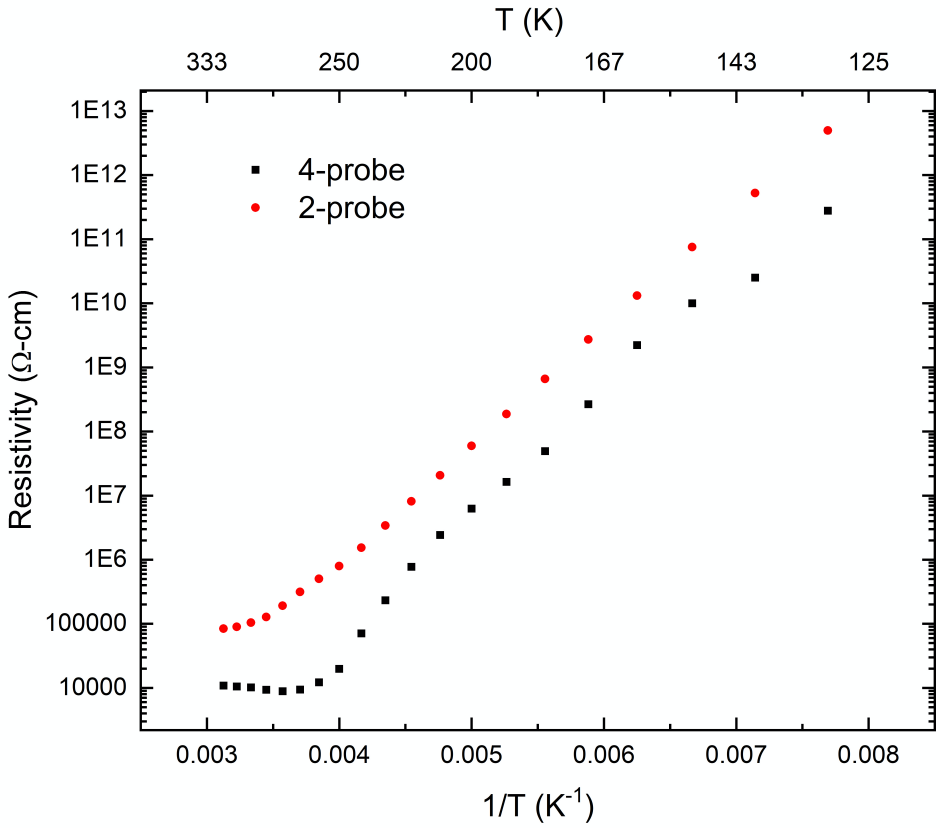

Fig. 6 — Two and four probe measurements of the temperature dependent resistivity of undoped Si.

Since previous studies of a possible 2D MIT in RuO_2 nano-skins were limited by the capabilities of our older PPMS, new samples were chemically synthesized and measured on this new system. The effects of disorder induced by calcination temperatures T = 300K to 400K in samples revealed a transition from 2D variable-range hopping (VRH) to Efros-Shklovskii ESVRH (a conduction model which accounts for the Coulomb gap, a drop in the density of states near the Fermi level due to interactions between localized electrons) to Arrhenius to 2D weak-localization was observed with increasing calcination temperature of single layer (10 nm) RuO_2 nanoskins Figure 7 shows the ESVRH part of the data.

A custom probe insert for the Dynacool system for performing temperature and magnetic field-dependent impedance spectroscopy at excitation current frequencies from DC to 3 GHz was also developed and tested. This will enable characterization of the frequency-temperature behavior of materials for future programs.

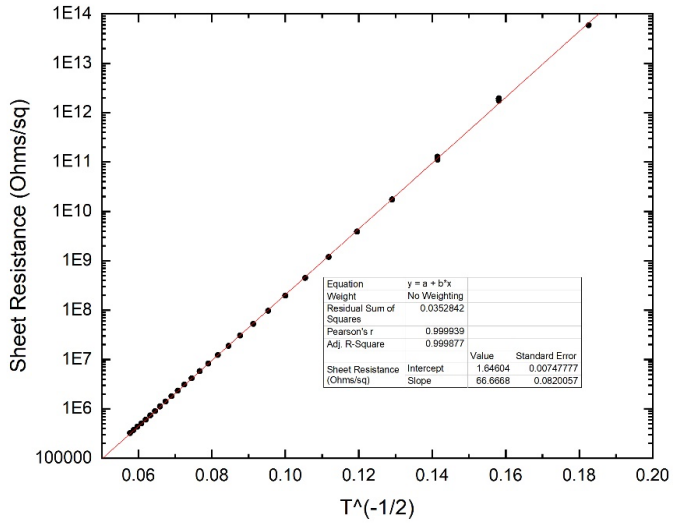

Fig. 7 — RuO_2 Nanoskin Single Layer (10 nm) on UHR sample platform following ESVRH, behavior.

5. CHARGE TRANSPORT MODELING NEAR METAL-INSULATOR TRANSITION

The discovery of high temperature superconducting (HTS) oxides has led to increased interest in the transport properties of oxide materials given the belief that an understanding of normal state properties is required to identify the mechanism behind HTS. Materials that do not behave as conventional metals have quasi-particles and well-defined Fermi surfaces. A generic account maps the electronic properties as a function of a doping parameter. Some highly doped materials that have no measurable superconductive transitions and exhibit Fermi liquid-like properties have resistivities that are generally higher than conventional metals. When the doping levels are reduced, superconductivity appears; the transition temperature T_c increases to a maximum value in the "optimally doped state" where the normal state properties are not consistent with Fermi liquid theory. One of the most striking examples is an apparent universal T^2 dependence of the cotangent of the Hall angle. As the doping is reduced further, the systems experience metal insulator transitions (MIT) on the so-called "under-doped" side of the phase diagram.

A simple "two-fluid model" (TFM) was developed to describe the normal state properties of materials near the MIT, in which two types of carriers, *localized* and *itinerant*, are separated by a mobility edge that defines the MIT. Crucially, the generation of itinerant carriers (characterized by a number density (n) occurs as temperature increases by thermal excitation from the localized part of the band. Since the properties of interest depend on n , their temperature dependence differs significantly from the usual metallic behavior. A description of this model, and its comparison to the usual generic representation of the electronic density of states (DOS) for simple metals, shows the separation into regions corresponding to conducting and insulating phases separated by a MIT.

For a simple metal, the number density n is found from the product of the density of states $D(E)$ with the Fermi Dirac distribution $f_{FD}(E)$ by

$$\mathrm{n} = \int_0^\infty D(E) f_{FD}(E) dE$$

$$D(E) = \frac{m}{\pi^2 \hbar^3} \sqrt{2mE} \equiv N_c \sqrt{E}$$

$$f_{FD}(E) = \left[1 + \exp\big(\beta(E-\mu)\big)\right]^{-1}$$

where the density of states (DOS) shown is for three dimensions, μ is the chemical potential, $\beta = k_B T$, and all other parameters have their conventional meanings. Representative cases of the integrand of n are shown in Figure 8.

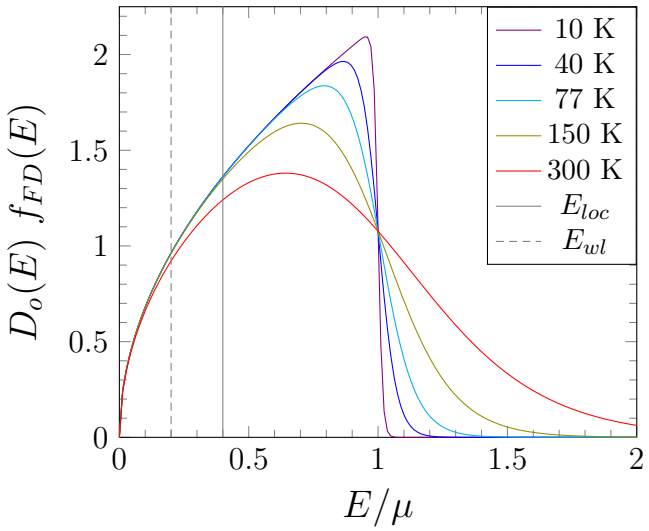

Fig. 8 — D(E) f_{FD}(E) for fixed μ = 0.5 eV for various temperatures. Position of E_{loc} and E_{wl} are for illustration only.more than one sentence. Two to three blank lines before and after each figure to separate from text.

For electrons in bulk, current density (taken to be in the $\hat{x}$ −direction) is

$$J_x = \frac{2q}{(2\pi)^3}\int dk_x \left(\frac{\hbar k_x}{m}\right)\int d\vec{k}_\perp f_{FD}(E_k)$$

Observing that $J = \sigma F$, $F = qE_F$ and E_F is the electric field in the $\hat{x}$ −direction and introducing

$$\delta_l[\beta(E-\mu)] \equiv \delta_l[s(E)] = f_{FD}(E)\big(1 - f_{FD}(E)\big)$$

where $s(E) = \beta(E-\mu)$, and the notation suggests the Dirac Delta function relation $\int_{-\infty}^{\infty}\delta_l(s)ds = 1$ results in the expression for conductivity

$$\sigma = \frac{2q^2}{3m}\beta\int_0^\infty ED(E)\tau(E)\delta_l[s(E)]\,dE$$

The function $\delta_l(s)$ is generally strongly peaked at the Fermi level so that

$$\sigma_{DC} \approx \frac{2q^2\tau(\mu)}{3\pi^2\hbar^3}(2m\mu^3)^{1/2} = \frac{q^2}{m}n_o\tau(\mu)$$

where $\hbar^2 k_F^2/2m =$ and $n_o \equiv k_F^3/(3\pi^2)$ (the zero-temperature number density for a metal), a well-known result.

The simplest form of the TFM alters the conductivity by changing the integrands in the variable range hopping and diffusive regimes and combining them in a prescribed manner. Redefine the scattering, diffusive, and variable range hopping contributions as

$$\sigma_\tau \to \frac{2q^2}{3m}\beta\int_{E_{loc}}^{\infty} ED(E)\tau(E,T)\delta_l[s(E)]\,dE$$

$$\sigma_{df} \to (\sigma_0 + \sigma_1 T^p)\int_{E_{loc}}^{\infty} \delta_l[s(E)]\beta dE$$

$$\sigma_{vr} \to \sigma_o e^{-(T_o/T)^p}\int_{0}^{E_{loc}} \delta_l[s(E)]\beta dE$$

where $s(E) \equiv \beta(E-\mu)$. The contributions of σ_τ, σ_{df}, and σ_{vr} are combined to find the total conductivity $\sigma(T)$ as follows. In the *metallic* phase,

$$\frac{1}{\sigma(T)} = \frac{1}{\sigma_\tau(T)} + \frac{1}{\sigma_{df}(T)}$$

which is equivalent to a sum of resistivities.

In the *insulating* phase,

$$\sigma(T) = \sigma_{vr}(T)$$

It is expected that at high temperature, σ_{df} will be overshadowed by σ_τ, given the temperature dependence of the former being $T^{1/2}$ and the later being characterized by the Bloch relation (T^5 for $T < T_D$): as a result, $\sigma_\tau^{-1} > \sigma_{df}^{-1}$ for temperatures that are high enough, thereby providing a means to extract the Bloch-dominated behavior for parameter evaluation. It can be shown that the entire range of data is reasonably well-approximated.

If σ_0, σ_1, and σ_o remain constant, but a non-zero E_{loc} is accounted for, the approximations become

$$\sigma_\tau \approx \frac{q^2}{m}\rho_o\tau(\mu)\frac{U_{3/2}(u,a)}{u^p}$$

$$\sigma_{df} \approx \left(\sigma_0 + \sigma_1 T^{1/2}\right)U_0(u,a)$$

$$\sigma_{vr} \approx \sigma_o e^{-(T_o/T)^{1/4}}U_0(u,-a)$$

where $u = \beta\mu, a \equiv \beta(E_{loc}-\mu)$ and $U_0(u,a)$ is the dimensionless conductivity integral.

The modification to the conductivities by weighting factors in the equations can model the doped $SrTiO_3$ data of Spinnelli, et al. [14], and is shown in Figure 9 compared to the analytic model. The purpose of the comparison is not to generate a highly accurate fit as before (indeed, the VR contributions have not been included, but to show that a single set of parameters (n_j, E_{loc}, ρ_e) are sufficient to qualitatively describe a wide range of conditions. The approximations to μ_j, on which the analytic model depends, are not expected to be quantitative (because they are linear fits to noisy parameters), but rather qualitative: even so, the agreement is *far better than expected* - even in the absence of considering the VR behavior - and

can be made even closer if “corrections" to the μ_j estimates are used, on which all the other analytic parameters depend.

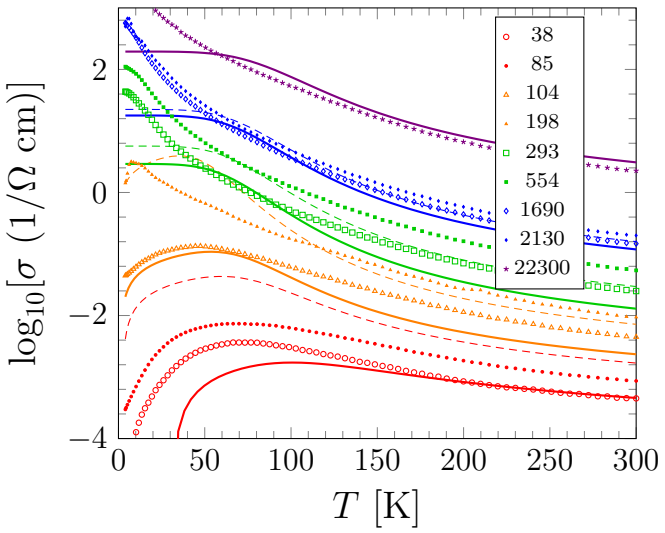

Fig. 9 — A comparison of the qualitative model (lines and dashed lines) using analytic forms for (T_D, C_j, σ_0, σ_1) compared to doped $SrTiO_3$ data of Ref. [14] (open and filled dots). Lines compare to open symbols of the same color; dashed lines compare to filled symbols of the same color. The units for the legend are 10^{14} cm^{-3}.

Using the relation $\partial_E f_{FD}(E) = -\beta\delta_l[s(E)]$, the longitudinal σ_E and transverse σ_H parts of conductivity can be written as

$$\sigma_E = \frac{\beta}{3}\int \frac{v^2 q^2 \tau \delta_l[s(E)]dk}{1+(\omega_c\tau)^2}$$

$$\sigma_H = \frac{\beta}{3}\int \frac{v^2 q^2 \tau \delta_l[s(E)](\omega_c\tau)dk}{1+(\omega_c\tau)^2}$$

where $\omega_c = qH/m$ is the cyclotron frequency. At low magnetic fields such that $\omega_c\tau \ll 1, letting\ v^2 = 2E/m$, then the conductivities can be written as

$$\sigma_E \to \frac{2q^2}{3m}\beta\int_{E_{loc}}^{\infty} E\, D_o(E)\tau(E) \sim \delta_l[s(E)]dE$$

$$\sigma_H \to \frac{2q^2}{3m}\beta\omega_c\int_{E_{loc}}^{\infty} E\, D_o(E)\tau(E)^2 \sim \delta_l[s(E)]dE$$

A numerical integration for σ_H can be implemented by a minor modification of the procedures developed for σ_E described previously, and therefore use can be made of the ratio

$$\frac{\sigma_H}{\sigma_E} = \omega_c \frac{\int_{E_{loc}}^{\infty} E D_o(E)\tau(E)^2\, \delta_l[s(E)]\mathrm{dE}}{\int_{E_{loc}}^{\infty} E D_o(E)\tau(E)\delta_l[s(E)]\mathrm{dE}}$$

For the degenerate case $\beta\mu \gg 1$ and $\mu > E_{loc}$,

$$R_H = \frac{1}{\rho q c}$$

$$\tanh \theta_H = \omega_c \tau(\mu)$$

Generally, however, μ need not be larger than E_{loc}. In such cases, then the Hall ratio can be rewritten using $s = \beta(E - \mu)$, and a and u as before. Then it becomes

$$\frac{\sigma_H}{\sigma_E} \approx \omega_c \tau(E_{loc}) \frac{\int_a^\infty f_2(s)\, \delta_l(s) ds}{\int_a^\infty f_1(s)\, \delta_l(s) ds}$$

$$f_n(s) = \left(1 + \frac{s}{u}\right)^{3/2} \left\{\frac{\tau[E(s)]}{\tau(E_{loc})}\right\}^n$$

Figure 10 shows a plot of $\cot(\theta_{Hall}) = \rho/\rho_{Hall}$ vs. T^2 resulting from the model which demonstrates that it can account for the unconventional behavior reported for various systems, including the HTS cuprates.

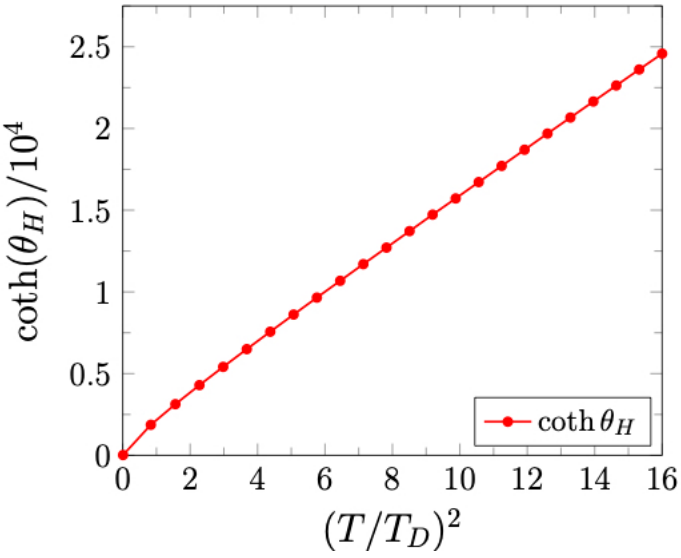

Fig. 10 — Model calculation of the temperature dependence of $\cot(\theta_{Hall})$ as a function of T^2.

6. CONCLUSIONS

The results of this program confirmed that conventional approaches to describing and predicting properties of functional materials with conductivities near the metal-insulator transition (MIT) must be complimented with those of the unconventional properties of the MIT. These include, superconductive, electronic transport, thermoelectric and electrocatalytic properties.

7. PUBLICATIONS

1. C. M. Krowne, "Critical Magnetic Field and its Slope, Specific Heat, and Gap for Superconductivity as Modified by Nanoscopic Disorder," Advances in Imaging and Electron Physics, Vol. 203, Academic Press, Elsevier, online, September 20, 2017.

2. A Ng, TE Sutto, BR Matis, Y Deng, PD Ye, RM Stroud, TH Brintlinger, Chemically exfoliating large sheets of phosphorene via choline chloride urea viscosity-tuning
Nanotechnology 28 (15), 155601, 2017.

3. E Breckenfeld, H Kim, EP Gorzkowski, TE Sutto, A Piqué, Laser-processing of VO_2 thin films synthesized by polymer-assisted-deposition. Applied Surface Science 397, 152-158 (2017).

4. C. M. Krowne, "Microscopic Field Effects at the NanoScale and Their Implications for Device Design in High-Speed Electronics," TC-11 Workshop: Advanced Materials and Their Characterization for EMC and High Speed Electronics, IEEE Intern. Symp. on Electromagnetic Compatibility, Signal Integrity and Power Integrity (EMC-SIPI), Long Beach Convention and Entertainment Center, Los Angeles (Long Beach), CA.,
July 30 – August 3, 2018; STRN: NRL/JA/6850-18-0011

5. C. M. Krowne**,** N. Cronk, and Xianwei Sha, "Calculation of Fundamental Physical Parameters for Lower Dimensional Materials," Computational, Biology, Chemistry and Materials Science (CCM), FY17 NRL DoD High Performance Computing Modernization Program Annual Reports, ed. P. A Shingler and B. A. Howell, Center for Computational Science, Information Technology Division, 58 – 59, Aug. 15, 2018; STRN: NRL/JA/6850-17-0096

6. C. M. Krowne, "Examination of 2D Hexagonal Band Structure from a Nanoscale Perspective for use in Electronic Transport Devices," An eleven chapter series, Advances in Imaging and Electron Physics, Vol. 210, 290 pages, Academic Press/Elsevier, online April 2019; STRN: NRL/JA/6850-18-0077

7. C. M. Krowne, "Physics of Ferroelectric Differential Capacitance Based Upon Free Energy, and Implications for Electronic Devices, J. Advanced Dielectrics 9, 1950002, 1 – 16, Jan. 21 2019; STRN: NRL/JA/6850-18-0094

8. C. M. Krowne, "Ferroelectric Differential Capacitance Affected by Stresses and Strains and Implications for Use in Electronic Devices, Microwave & Opt. Tech. Lett. 61, 948 - 953, Jan. 2019; STRN: NRL/JA/6850-18-0080; **DOI:** 10.1002/mop.31699

9. E. M. Clements, R. Das, M. Phan, L. Li, V. Keppens, D. Mandrus, M. Osofsky, H. Srikanth**,** Magnetic field dependence of nonlinear magnetic response and tricritical point in the monoaxial chiral helimagnet $Cr_{1/3}NbS_2$, PHYSICAL REVIEW B **97,** 214438 (2018); **DOI:** 10.1103/PhysRevB.97.214438

10. J. Wu, B. Gautam, M. A. Sebastian, V. Ogunjimi, S. Misra, J. J. Huang, J. Baca, J. Prestigiacomo, T. Haugan, H. Y. Wang, M. Osofsky, **"**Pinning Efficiency of One-Dimensional Artificial Pinning Centers in $YBa_2Cu_3O_{7-x}$ Thin Films," IEEE TRANSACTIONS ON APPLIED SUPERCONDUCTIVITY **29**, 8001105 (2019) **DOI:** 10.1109/TASC.2019.2895739

11. V. N. Smolyaninova, J. W. Lynn, N. P. Butch, H. Chen-Mayer, J. C. Prestigiacomo, M. S. Osofsky, I. I. Smolyaninov, "Observation of plasmon-phonons in a metamaterial superconductor using inelastic neutron scattering," Phys. Rev. B, **100**, 024515 (2019).

12. V. N. Smolyaninova, W. Korzi, W. Zimmerman, S. Searfoss, C. Jensen, G. Yong, D. Schaefer, J. C. Prestigiacomo, M. S. Osofsky, H. Kim, Z. Xing, M. M. Qazilbash, I. I. Smolyaninov, "Superconducting properties of tin-based ENZ and hyperbolic metamaterials," Physica C **565**, 1353511 (2019).

13. K.L. Jensen, J.M. Connelly, J.J. Petillo, J.R. Harris, S. Ovtchinnikov, A.J. Jensen, J. Burke, M. Cahay, J. Ludwick, G. Tripathi, J. Sanchez-Roddy, and D. Puentes, "Semi-analytic model of a carbon fiber thermal-field emitter," J. Appl. Phys. **129**, 095107 (2021). https://doi.org/10.1063/5.0044800.

14. P. F. Rosen, J. J. Calvin, and B. F. Woodfield, V. N. Smolyaninova, J. C. Prestigiacomo, M. S. Osofsky, and I. I. Smolyaninov, "Normal state specific heat of a core-shell aluminum-alumina metamaterial composite with enhanced T_c," Phys Rev B **103**, 024512 (2021), DOI: 10.1103/PhysRevB.103.024512.

15. L. Holleis, J. C. Prestigiacomo, Z. Fan, S. Nishimoto, M. Osofsky, G.-W. Chern, J. van den Brink, and B. S. Shivaram, "Anomalous and anisotropic nonlinear susceptibility in the proximate Kitaev magnet α-$RuCl_3$," npj Quantum Materials 6:66 (2021)6:66. https://doi.org/10.1038/s41535-021-00364-z

16. C. M. Krowne and X. Sha, "Atomic structural and electronic band structure calculations for borophene," Mater. Res. Express (IOP) **8**, 026301 (2021).

17. C. M. Krowne, "Graphyne and Borophene as Nanoscopic Materials for Electronics - with Review of the Physics," Adv. Imaging Electr. Phys. **218**, 159 (2021). https://doi.org/10.1016/bs.aiep.2021.04.003.

18. V.N. Smolyaninova, W. Korzi, G. Yong, A.-M. Valente-Feliciano, D. R. Beverstock, J. C. Prestigiacomo, M. S. Osofsky, I. I. Smolyaninov, "Effect of metamaterial engineering on the superconductive properties of ultrathin layers of NbTiN," J. Appl. Phys. **130**, 073901 (2021).

8. PATENTS

1. Purification of coal and fly ash by ionic liquids TE Sutto US Patent 9,637,832

2. Synthesis of unit cell sized oxide particulates, TE Sutto US Patent 9,580,319

3. Method of Making a Concentrated Metal Salt Solution in a Non-Aqueous Solvent System, TE Sutto US Patent App. 15/645,906. (2018)

9. PRESENTATIONS

1. "Application of metamaterial nano-engineering for increasing the superconducting critical temperature," M. Osofsky, National University of Singapore, Singapore, 30 July 2018

2. "Application of metamaterial nano-engineering for increasing the superconducting critical temperature," M. Osofsky, 12th International Conference on Ceramic Materials and Components for Energy and Environmental Applications (CMCEE 2018), Singapore, 26 July 2018; STRN: 17-1231-1274

3. “Application of metamaterial nano-engineering for increasing the superconducting critical temperature,” Applied Superconductivity Conference, 28 Oct - 2 Nov 2018

4. “Application of metamaterial nano-engineering for increasing the superconducting critical temperature,” M. Osofsky, Electronic Materials and Applications 2019, Orlando, Florida, 23-25 Jan 2019; STRN: 17-1231-1274

5. “Enhanced T_c Near the Metal/Insulator Transition: a New Tool in The Search for Superconducting Materials,” Stanford University, Palo Alto, CA, 21 May 2019

6. “Application of metamaterial nano-engineering for increasing the superconducting critical temperature,” Energy Materials Nanotechnology Quantum Meeting, Barcelona, Spain, 19-23 August 2019

7. “Application of metamaterial nano-engineering for increasing the superconducting critical temperature,” University of Cambridge, Cambridge, UK, 16 August 2019

8. “Use of PCAR to measure the transport spin polarization of Pt/ferromagnetic insulator bilayers,” 2018 Conference on Electronic and Advanced Materials, Orlando, FL, 22-24 Jan 2020

9. “Use of PCAR to measure the transport spin polarization of Pt/ferromagnetic insulator bilayers,” Towson, MD, 21 Feb 2020

10. "Use of PCAR to measure the transport spin polarization of Pt/ferromagnetic insulator bilayers", virtual Applied Superconductivity Conference, 24 Oct-7 Nov, 2020

11. "Use of PCAR to measure the transport spin polarization of Pt/ferromagnetic insulator bilayers-Evidence for the Magnetic Proximity Effect", virtual Fall Meeting of the Materials Research Society, 27 Nov-4 Dec, 2020

12. “Metal-insulator transition in two dimensional systems”, Towson University, Towson, MD 4 Feb 2022

REFERENCES

1. M. S. Osofsky, R. J. Soulen, Jr., J. H. Claassen, G. Trotter, H. Kim, and J. S. Horwitz, “Enhanced superconductivity in metallic oxides near the metal-insulator transition,” Phys. Rev. B **66**, 020502(R) (2002).

2. V. N. Smolyaninova, B. Yost, K. Zander, M. S. Osofsky, H. Kim, S. Saha, R. L. Greene, I. I. Smolyaninov, “Experimental demonstration of superconducting critical temperature increase in electromagnetic metamaterials,” SCIENTIFIC REPORTS, **4**, 7321 (2014).

3. V. N. Smolyaninova, K. Zander, T. Gresock, C. Jensen, J. C. Prestigiacomo, M. S. Osofsky, I. I. Smolyaninov, “Using metamaterial nanoengineering to triple the superconducting critical temperature of bulk aluminum,” SCIENTIFIC REPORTS, **5**,15777 (2015).

4. Vera N. Smolyaninova, Christopher Jensen, William Zimmerman, Joseph C. Prestigiacomo, Michael S. Osofsky, Heungsoo Kim, Nabil Bassim, Zhen Xing, Mumtaz M. Qazilbash & Igor I. Smolyaninov,

"Enhanced superconductivity in aluminum-based hyperbolic metamaterials," SCIENTIFIC REPORTS, **6**, 34140 (2016).

5. Osofsky, M.S.; Krowne, C.M; Charipar, K.M.; Bussman, K.; Chervin, C.N., Pala, I.R.; Rolison, D.R. SCIENTIFIC REPORTS **6**, 21836 (2016).

6. Chervin, C.N.; Lubers, A.M.; Pettigrew, K.A.; Long, J.W.; Westgate, M.A.; Fontanella, J.J.; Rolison, D.R. *Nano Letters*, **9**, 2009, 2316-2321.

7. Chervin, C.N.; Lubers, A.M.; Long, J.W.; Rolison, D.R. Journal of Electroanalytical Society, 644, 2010, 155-163.
8. Lytle, J. C.; Rhodes, C.P.; Long, J.W.; Pettigrew, K.A.; Stroud, R.M.; Rolison, D.R. Journal of Materials Chemsitry, 17, 2007, 1292-1299.

9. Ryan, J. V.; Berry, A. D.; Anderson, M. L.; Long, J. W.; Stroud, R. M.; Cepak, V. M.; Browning, V. M.; Rolison, D. R.; Merzbacher, C. I. Nature 2000, 406, 169−172.

10. DeSario, P.A.; Chervin, C.N.; Nelson, E.S.; Sassin, M.B.; Rolison, D.R. ACS Applied Materials and Interfaces, 9, 2017, 2387-2395.

11. Donakowski, M.D.; Mansour, A.N.; Pala, I.R.; Chervin, C.N.; DeSario, P.A.; Long, J.W.; Rolison, D.R. J. Phys. Chem. C. 122, 2018, 28895-28900.

12. Music, D.; Basse, F.; Han, L.; Devender; Borca-Tasciuc, T.; Gengler, J.J.; Voevodin, A.A.; Ramanath, G.; Schneider J.M. Appl. Phys. Lett. 104, 2014, 053903.

13. Music, D.; Basse, F.; Habdorf, R.; Schneider, J.M. Journal of Applied Physics, 108, 2010, 013707.

14. A. Spinelli, M. A. Torija, C. Liu, C. Jan, and C. Leighton, Phys. Rev. B 81, 155110 (2010).